Supporting Information

Gas-phase Chemistry of Actinides Ions: New Insights into the Reaction of UO^+ and UO^{2+} with Water

Maria del Carmen Michelini, Nino Russo*, Emilia Sicilia

Dipartimento di Chimica and Centro di Calcolo ad Alte Prestazioni per Elaborazioni Parallele e Distribuite-Centro d'Eccellenza MURST, Università della Calabria, I-87030 Arcavacata di Rende, Italy

* Email: nrusso@unical.it

Table of Contents

c. Figure S3: ELF localization domains (η = 0.6) for the lowest-energy spin state species involved in the $UO^{+2} + H_2O$ reaction pathway (Path A).
d. Figure S4: ELF localization domains (η = 0.6) for the lowest-energy spin state species involved in the $UO^{+2} + H_2O$ reaction pathway (Path B).

1 Bonding analysis

The characteristics of the bonding of all the key minima and transition states found along the reaction pathways were studied within the framework of topological metodologies. In particular, we have used the topological analysis of the electron localization function (ELF) as proposed by Silvi and Savin.[1] The fundaments and applications of this method to the understanding of the chemical bond and the bonding evolution along reaction pathways are well documented. Recent works demonstrate that this method is a reliable tool to analyse the nature of the chemical bonds present in systems containing transition metals.[2]

ELF calculations were carried out with TopMod package developed at the Laboratoire de Chimie Théorique de l'Université Pierre et Marie Curie.[3] Graphical representations of the bonding were obtained by plotting isosurfaces of the localization functions by using the public domain scientific visualization and animation program Molekel.[4]

Bonding and electronic properties were also explored using AIM techniques.[5] In particular, we report the main properties of the (3,-1) bond critical points (bcp) in the gradient field of the electron density. The bcp were primarily localized with the EXTREME program (part of the AIMPAC package)[5] and verified with TopMod program.

Furthermore, atomic charges calculated within Natural Population Analyses (NPA) and bonding description from Natural Bond Orbital (NBO) scheme are also reported.[6] In a recent theoretical work,[7] different valence/Rydberg partitions were applied to different uranium-containing species, and it was concluded that NPA performs well after modification of the partitioning of atomic orbitals to include the 6d AO in the valence space. Therefore, here we present two different results for NPA analysis,

firstly we have performed the NBO analysis by using the default AOs partition of Gaussian03 package. This partition includes 7s and 5f orbitals in the valence space whereas the 8-10s, 7-10p, 6-9d, 6f and 7f orbitals are included in the Rydberg space. We have performed the same analysis by using a modified version of Gaussian program that includes the 6d orbitals into the valence space. We have found that the most positive uranium charges are obtained when using the default AOs partition. That values are systematically higher than AIM charges. On the contrary, the modified partition yields much less positive charges, being in all cases smaller than the corresponding AIM charges.

In Tables S1 to S4 are collected the average electron basin populations, ($\bar{N}_i$), the integrated spin densities, $<S_Z>$, and the relative fluctuations, $\lambda(\bar{N}_i)$, of all the lowest-energy spin state species involved in the studied reactions. The ELF (η) localization domains (isosurfaces of $\eta = 0.60$) of all the species involved in $UO^+ + H_2O$ and $UO^{2+} + H_2O$ paths are displayed in Figures S1-S4.

Bonding properties derived from the electron density, ρ, and its gradient are gathered in Tables S5 to S8. In particular, we report the electron density at the bcp, ρ(bcp), and the second derivative or Laplacian of the density, $\nabla^2\rho$(bcp), which measures the extend to which density is concentrated or depleted (more negative $\nabla^2\rho$(bcp) indicates greater concentration of charge).

In a previous theoretical work,[7] it was reported a notably large atomic volume for U(VI), in particular, in the case of UO_2^{2+} that volume was found to be larger than that of O^{2-}, with an atomic radii ratio of 1.27. We have calculated the atomic radii ratio (r_c/r_a) for all the cationic uranium oxides studied in this work, in order to analyse the trend in a series of oxides that have different formal oxidation numbers, i.e. $U(III)O^+$, $U(IV)O^{2+}$, $U(V)O_2^+$, and $U(VI)O_2^{2+}$ (Table S9). We have calculated that ratio from the bond critical point position along the U-oxo axis as well as directly from the AIM basin volumes obtained from TopMod package. The radii ratio calculated from the AIM basin volumes could be defined as the radius of a sphere of volume equal to that of the atomic basin, being in this way an average property. It is interesting to note, that in the case of the radii ratio obtained from the position of the U-O BCPs we have found a systematic decreasing of that property from UO^+ to UO_2^+, as expected from the increasing formal oxide number (Table S9). This trend is broken off by an important increase

of that relation in the case of UO_2^{2+}. These results therefore, agree with the results reported in ref. 7. The "averaged" radii ratio obtained from the AIM basin volumes, follows the same trend, even when in this case the increase of the calculated radio for UO_2^{2+} is much less marked.

Tables S10 and S11 show the NPA charges and the natural valence populations (for uranium atom) of all the species involved in the $UO^+ + H_2O$ reaction pathway (in their ground spin states), obtained with the default partition of the Valence/Rydberg space and with the modified partition, respectively. Tables S12 and S13 report the same data for the $UO^{2+} + H_2O$ reaction path. In Tables S10 and S12 we have included the uranium atomic charges calculated within the AIM theory framework. The AIM theory provides a definition of atomic charges that is completely different from any other orbital-based population analysis. Atomic charges are obtained in this case by integration of the electron density within the atomic basins and adding the nuclear charges.

1.1 UO^+ and UO^{2+}

We will firstly describe and compare the bonding characteristics of the uranium monoxides, UO^+ ($^4\Delta$) and UO^{2+}($^3\Sigma_g$). ELF analysis indicates that both oxides are characterized by the presence of a disynaptic valence basin V(U,O) with a population of 7.47 electrons (UO^+) and 7.19 electrons (UO^{2+}), respectively. A special feature of both oxides is that the maximum corresponding to the V(U,O) attractor is found to be behind the O atom, being the basin population located mostly at the oxygen atomic basin. Such features, which are common for lone pairs, are an indication of the high ionic character of the U-O bond. This fact is further evidenced by the low values of the metal contribution to that disynaptic valence basins (this contribution is labeled as V(U,O)|U in Tables S1 and S3).

The integrated spin density is almost fully localized in the C(U) and V(U) basins. From three unpaired electrons in UO^+, one is localized at the core basin and two at the monosynaptic valence basin, whereas in the case of UO^{2+}, one unpaired electron is localized at the core and the second one at the monosynaptic valence basin, V(U) (see $<S_z>$ values in Tables S1 and S3).

For all the species involved in the reaction paths, the average population ($\bar{N}_i$) of the metallic core basins, C(U), has a value betweeen 17.5 and 18.0 electrons, with few exceptions. Considering that we are using an effective core potential that includes 60 electrons ([Kr] + 4d and 4f electrons), the 18 electrons corresponds mostly to the 5s, 5p and 5d electrons, as confirmed by the analysis of the orbitalic contribution to the C(U) basin population. The uranium contribution to the V(U,O_1) basin has a mixed p-d-f character, whereas the oxygen atom contributes to the same basin with p- and s-type electrons.

The variance (σ^2) of the population of C(U) basin is very large, typically of the order of 3.2 electrons. The covariance analysis shows that the delocalization mostly involves the V(U) monosynaptic basins (around 90 % of σ^2), and to a lesser extent the monosynaptic V(O) basins. This is an indication of a large electron fluctuation between the metallic basins.

An analysis of the bond critical points of the gradient vector field of the charge density (AIM analysis), indicates that the bcp located betwen the uranium and oxygen atoms in UO^+ ($^4\Delta$) has a value of ρ(bcp) of 0.272 a.u., whereas $\nabla^2\rho$(bcp) amounts 0.393 a.u. Similar properties were found in the case of UO^{2+} ($^3\Sigma_g$) (Tables S5 and S7). Therefore, while ρ(bcp) is quite large, the Laplacian at the bcp is positive, indicating that charge is concentrated in the separated atomic basins rather than in the internuclear region, which is thus locally depleted of electronic charge. Within AIM framework, such an interaction has been termed “intermediate” between shared and closed-shell interactions, where the later exhibits a low value of ρ(bcp) associated to a positive Laplacian.

The picture of the bonding provided by ELF and AIM analysis is not contradicted by NBO analysis, which in the case of UO^+ ($^4\Delta$) indicates the presence of three molecular orbitals between uranium and oxygen. The main contribution to these orbitals comes from the oxygen atom, which in the case of the σ -bond, contributes in an 80.82% to that natural orbital. The s-p hybrid of oxygen has a 95% of p-character, and is therefore mostly formed from p orbitals. Both π-type natural orbitals are formed from an d-f uranium hybrid (50% d-character, 50 % f-character), and pure p oxygen orbitals. The polarization coeficients (0.36 for U and 0.93 for O) indicates that oxygen with a 86.71 % has the

larger percentage of this NBO. In the case of UO^{2+} ($^3\Sigma_g$) the characteristics of the bonding are quite similar, the σ-orbital is formed from an almost pure p oxygen orbital (95.78 % p) and a p-d-f uranium hybrid (5.41 % p, 23.87 %d and 70.18 %f), being the polarization coeficients 0.85 for oxygen and 0.54 for uranium. The π-type natural orbitals are formed from d-f uranium hybrids (38.85 % f and 61.14 %d). The unpaired electrons in UO^{2+} (triplet state) are located in nonbonding δ orbitals that arise from the 5f uranium orbitals, whereas in the case of UO^{2+} in its singlet state there is a lone pair located in a δ_u orbital. In UO^+ (quartet state) two of the unpaired electrons are located in nonbonding δ_u orbitals, whereas the third one has a σ character.

NBO results could be interpreted to describe the U-O bond as strongly polarized towards oxygen atom and mostly ionic in nature. The NBO qualitative description of the U-O bond is fairly maintained over all the species along the paths, with only some slight variations in the relative atomic contributions to that bond. Consequently, we do not further report the details of that analysis in next sections.

1.2 UO^+- H_2O and UO^{2+}- H_2O

The ELF topological analysis of these complexes indicates that there is no covalent bond formation between the fragments, as evidenced by the absence of a disynaptic valence basin between uranium and the water oxygen atom (see Tables S1 and S3). We should note that in the case of the UO^+-H_2O complex, there is some redistribution of charge between the different UO^+ basins, namely, there is an important increase of the V(U) basin population (almost 1 electron) at expenses of the C(U) basin, whereas the disynaptic $V(U,O_1)$ basin, which represents the U-O uranium monoxide bond, has a slightly lower population mostly due to a diminishing of the uranium contribution to that basin. In the case of UO^{2+}-H_2O instead, the ELF analysis does not indicate important variations with respect to the separated fragments. Therefore, the interaction between UO^+ and UO^{2+} with H_2O in the first complex corresponds physically to an electrostatic interaction. These results agree with AIM analysis, which shows the presence of a (3,-1) bcp between U and O(2) atoms, with a very low charge density, namely,

ρ(bcp) = 0.048 a.u. in the case of UO^{+}-H_2O, and 0.062 a.u. for UO^{2+}-H_2O. In both cases $\nabla\rho$(bcp) is positive (see U-O(2) bond in Tables S5 and S7).

This picture also agrees with the description of the bonding found by using the NBO approach, which indicates only the presence of the O-H bonds of water, and the U-O(1) bond, with the same characteristics of the previously described bare oxides.

1.3 TS1 and TS1'

The ELF topological analysis of these structures shows that in both cases the first O-H bond breaking takes place at this stage of the reaction. This fact is evidenced by the lack of the $V(O_2,H_1)$ basin (see Tables S1 and S3) which is replaced by a trisynaptic $V(H_1,U,O_2)$ basin with a population of 1.11 electrons (0.98 in the case of TS1'). In both structures, therefore, the H atom belongs to a three-centered bond. We note, however, that the atomic electron contribution to that basin population comes mostly from H atom, being the contribution of U and O atoms quite small (around 10 % of the total basin population). There is an important spreading of the spin density as a consequence of the topological changes that take place in these transition structures (see $<S_z>$ values in Tables S1 and S3).

The disappearance of the disynaptic $V(O_2,H_1)$ basin, provokes also some redistribution of charge between the rest of the basins that involves that O atom (i.e. $V(O_2)$ and $V(O_2,H_2)$). On the other side, there is a slight increase in the population of the disynaptic $V(U,O_1)$ basin, due to a higher contribution coming from U atom (see $V(U,O_1)|U$ in Table S1). The strong lowering of the ρ(bcp) and the change of sign of the Laplacian at the bcp corresponding to the O(2)- H(1) bond, indicates that the broken of the first O-H bond at this stage of the reaction is also supported by the AIM analysis (Tables S5 and S7). According to ELF, the U-O(2) bond is not yet formed. However, there is an important increase in the electronic density of the corresponding bcp, which continues to grow through all the structures involved in the reaction paths, to arrive up to the same ρ(bcp) value of U-O(1) bcp in the second insertion intermediate (see Tables S5 and S7).

The formation of the first transition state, involves a charge transfer from the U atom to the hydrogen atom that is being tranfered ($q(H_1)$ in Tables S10-S13). As a consequence, the charge on the metal center increases up to +2.64 (2.21) for TS1 and +2.92 (2.54) for TS1', according to the NPA analysis using the default (modified) atomic orbital partition.

1.4 HUO_2H^+ and HUO_2H^{2+}

The formation of the first insertion intermediate, provokes a further redistribution of charge and important topological changes. ELF analysis shows that in HUO_2H^+ the trisynaptic valence basin dissapears, being replaced by a disynaptic $V(H_1,U)$ valence basin, with a population of 1.69 electrons. This is an indication of the formation of a U-H covalent bond. The contribution of electron population coming from U atom is of around 20 % of the total basin population. The low integrated spin density of the $V(H_1,U)$ basin of HUO_2H^+ clearly confirms the presence of the coupled spin pair.

This view is supported by AIM analysis, which indicates the presence of a (3,-1) critical point between U and H atoms, with a negative value of the Laplacian of the charge density(see Table S5).

In the case of HUO_2H^{2+} the trisynaptic basin is replaced by a monosynaptic $V(H_1)$ basin with a population of 0.91 electrons. The integrated spin density concentrated on that basin confirms that it is populated basically by one electron. This description clearly agrees with the results of AIM analysis, which indicates that the charge density at the U-H bcp is more than five times smaller than the corresponding value for the monopositive intermediate, and has a positive $\nabla^2\rho$(bcp) value (Table S7).

We note that in the case of HUO_2H^+ the spin-crossing has already taken place and the system is already in its low spin state whereas the dicationic moiety is still in its triplet (high-spin) state. The rest of the basins shows only slight variations with respect to the previous transition structures. The merge of the V(O) monosynaptic basins is a consequence of the symmetry change of the species.

The charge on the metal center is further increased. The NPA charge is +2.85 (2.23) in the case of HUO_2H^+ and +3.02 (2.59) in HUO_2H^{2+}; for the default (modified) valence space. Considering the natural charge distribution in both intermediates we note that in the case of HUO_2H^+ structure, the H

atom being transferred is negatively charged, whereas in the case of HUO_2H^{2+} the charge on that atom is only slightly positive, which is consistent with the topological differences found in that structures.

1.5 TS2 and TS2'

According to ELF analysis at this stage of the reactions the formation of the second U-O covalent bond takes place, as shown by the presence of the $V(U,O_2)$ valence basin, mostly formed from the charge transfer coming from $V(O_2)$ monosynaptic basins, which are absent in these structures. The electron population of the $V(U,O_2)$ basins are lower than the $V(U,O_1)$ population by almost an electron, in the case of TS2. There is an important increase of the charge density at the U-O(2) bcp, even when that value is still lower than the density at the U-O(1) bcp (Table S5 and S7). In TS2' the monosynaptic $V(H_1)$ basin dissapears, being replaced by a disynaptic $V(H_1,U)$ valence basin with a population 1.47 e, which represents the formation of a covalent bond between the U atom and the firstly transfered H atom (H_1). The electronic contribution of uranium to the $V(H_1,U)$ valence basin is quite small (around 12 % of the basin population). The population of the $V(H_1,U)$ basin in TS2 is slightly higher (1.66 electrons). The contribution of the metal atom to the total electronic population is of 10 % (see $V(H_1,U)|U$ in tables S1 and S3). Both structures are at this stage in their lowest spin state.

The second O-H bond is not yet completely broken, as evidenced by the existence of the $V(O_2,H_2)$ basin, which has a very low electron population (0.65 e in TS2 and 0.61 e in TS2'). This is an indication of the strong weakening of this bond. This fact is supported by the important diminishing of the O(2)-H(2) ρ(bcp) (Tables S5 and S7).

1.6 $(H_2)UO_2^+$ and $(H_2)UO_2^{2+}$

The ELF analysis of these reaction intermediates shows the lack of two disynaptic valence basins, $V(H_1,U)$ and $V(O_2,H_2)$. This indicates that the U-H(1) and O(2)-H(2) covalent bonds are completely

broken at this step, giving place to the formation of a disynaptic $V(H_1,H_2)$ basin, with an electron population very close to two electrons. Comparing the basin populations of $(H_2)UO_2^+$ and $(H_2)UO_2^{2+}$ with the corresponding cationic uranium dioxides, it is evident that the H_2 bond is already formed and that the structures can be considered as formed by two fragments, UO_2^+ (or UO_2^{2+}) and H_2. The ELF description of the second insertion intermediate is supported by the AIM analysis, which shows that the charge density and the Laplacian values for the H(1)-H(2) bcp are comparable to the corresponding values for the free H_2 molecule. The same properties for the U-O bcp are comparable to those corresponding to the bare UO_2 cationic oxides (see Tables S5 and S7).

1.7 UO_2^+ and UO_2^{2+}

The electronic structure and bonding properties of uranyl ion have been widely studied in the last years.[7,8] The ground state of UO_2^+ is a $^2\Phi_u$, with an unpaired 5fϕ electron, whereas UO_2^{2+} ground state is a $^1\Sigma_g^+$ with no unpaired electrons on the metal. The main features that characterize the bonding of both dioxides is the presence of two disynaptic valence basins, $V(U,O_1)$ and $V(U,O_2)$, each one with a population of around 7.40 electrons (Tables S1 and S3). As in the U-O bonds of the previously described structures, the main contribution to these basins comes from oxygen atom (about 90 %) indicating the presence of a covalent bond with a strong ionic character.

An analysis of the (3,-1) bond critical point properties gives also a clear indication of the high ionic nature of the bonds. In particular, for UO_2^+ ($^2\Phi_u$) the value of ρ(bcp) at this point is 0.314 and $\nabla^2\rho$(bcp) is 0.234 a.u., whereas in UO_2^{2+} system the corresponding values are 0.368 and 0.284 a.u. Based on AIM charges, the U atom bears a partial charge of +2.69 elementary charges in UO_2^+ and +3.20 in UO_2^{2+}. The corresponding values obtained with NPA, are +2.79 (2.33) and 3.30 (2.83) for the default (modified) partition of the valence space. We note that the metal charge increases along the reaction path up to reach the maximum values in the dioxides. The description of the U-O bond from NBO analysis shows that the characteristics of these bonds are similar to the previously described for the monoxides. For instance, in the case of UO_2^{2+}, the σ-type bond is formed from an sp hybrid (91.08

% p-character) and an sdf metal hybrid (11.10 % s, 40.17 % d and 48.60 % f), with a polarization coeficient (0.86) that clearly shows the larger contribution of oxygen to this NBO (74.42%). The π-type natural bonds are formed from d-f uranium hibrids orbitals (50%d, 50%f), and pure p oxygen orbitals.

1.8 Species involved in Path B: TS3 and TS3'

The main feature of these structures is the presence of a detached hydrogen atom, as evidenced by the existence of a monosynaptic valence basin, $V(H_2)$, with a population of around 0.37 electrons (Tables S2 and S4, Figures S2 and S4). That indicates that the proton transfer occurs in a two-step process involving the breaking of a O-H and the formation of the new O-H bond. This type of mechanism that involves a so-called "dressed proton" have been previously described in detail.[9] Two disynaptic basins are present, namely, the $V(O_2,H_1)$ which indicates the presence of an O-H covalent valence bond, and the $V(O_1,U)$ basin with a population of 6.30 electrons. The characteristics of the U-O bond are similar to the previous described structures, namely most of the electronic population of the $V(O_1,U)$ comes from the oxygen atom, whereas the contribution of the metal atom is really very low, namely around 3%. We note the lack of the second U-O bond (see Tables S2 and S4).

AIM analysis for these species, indicate the presence of a (3,-1) bcp between the U-O(2) with a quite low ρ(bcp), namely ρ(bcp) = 0.077 a.u. (0.113 in the case of the dicationic species). In the case the U-O(1) bond that values are quite higher. In all cases $\nabla^2\rho$(bcp) is positive. Another three (3,-1) bcp were localized. Firstly, between the O(2)-H(1) atoms the topological properties are very close to that of an O-H bond in H_2O molecules, whereas between the second hydrogen atom, H(2) and each oxygen atom, we have located a (3,-1) bcp with much lower ρ(bcp) and $\nabla^2\rho$(r). In both cases $\nabla^2\rho$(r) is negative.

1.9 Species involved in Path B: $U(OH)_2^+$ and $U(OH)_2^{2+}$

ELF analysis indicates that both bis-hydroxides are characterized by the presence of two O-H covalent bonds. There are no disynaptic valence basins between the U atom and the oxygen atoms. Therefore, the interaction between the U atom an the O-H fragments, is mainly electrostatic. The rest of the basins present in these structures correspond to monsynaptic valence basins of U and O atoms.

AIM analysis for these species indicates the presence of (3,-1) bcps between the U-O atoms with values of the charge density that are half of the corresponding values in the bare monoxides, whereas $\nabla^2\rho(r)$ is large and positive. The AIM properties for the O-H bonds are similar to that values in the H_2O molecule. In the case of the monocationic moiety the AIM charge on the metal atom is +2.25 e, whereas the NPA value is +2.47 (2.18) for the default (modified) partition of the valence space. The corresponding values for the dicationic species are +2.82 (AIM), +3.05 and +2.70 for the default and modified NPA.

1.10 Species involved in Path B: TS5 and TS5'

According to ELF analysis, these moieties are characterized by the presence of a trisynaptic $V(H_1,U,O_2)$ valence basin with an electronic population of 1.22 electrons (0.93 e in the case of the dicationic species). This is an indication that the hydrogen atom being transfered to the metal center, is involved in a three-center two-electrons bond. However, around 80 % of that basin population comes from H atom. The presence of a disynaptic valence basin between one of the oxygen atoms and the metal atom, indicates that there is a bonding between that atoms. However, as in the previous cases, the contribution from the metal atom to the population of that basin is extremely low, namely around 3 % of the total population.

We have localized three (3,-1) bcps in these structures (see Tables S6 and S8). There is an important increase of the charge density at the U-O(2) bcp, with respect to the previous minima. We note that

between the O(2)-H(1) atoms the ρ(bcp) values are notably low, whereas the $\nabla^2\rho(r)$ are small and positive.

ACKNOWLEDGMENT Financial support from the Università degli Studi della Calabria is gratefully acknowledged. We kindly thank Dr. Sandro Chiodo for his advice into the implementation of the modified version of Gaussian03 program.

2 References

(1) (a) Becke, A. D.; Edgecombe, K. E.; *J. Chem. Phys.* 1990, *92*, 5397. (b) Silvi, B.; Savin, A. *Nature* 1994, *371*, 683.

(2) See for instance (a) Calatayud, M.; Silvi, B.; Andrés, J.; Beltrán Chem. Phys. Lett. **2001**, *333*, 493. (b) Pilme, J.; Silvi, B.; Alikhani, M. E. *J. Phys. Chem. A* **2003**, *107,* 4506. (c) Michelini, M.C.; Sicilia, E.; Russo, N.; Alikhani, M. E.; Silvi, B. *J. Phys. Chem. A* **2003**, *107,* 4862. (d) Chiodo, S. ; Kondakova, O.; Michelini, M.C.; Russo, N.; Sicilia, E.; *J. Phys. Chem. A* **2004**, *108,10*69. (e) Michelini, M.C.; Russo, N.; Alikhani, M. E. Silvi, B.; *J.Comput. Chem.* **2004**, *25*, 1647. (f) Chiodo, S. ; Kondakova, O.; Michelini, M.C.; Russo, N.; Sicilia, E.; *Inorg.Chem.* **2003**,*42, 8773*. (g) Michelini, M.C.; Russo, N.; Sicilia, E.; *Inorg.Chem.* **2004**, *43, 4944*. (h) Michelini, M.C.; Russo, N.; Alikhani, M. E. Silvi, B.; *J.Comput. Chem.* **2005**, *26*, 1284. (i) Petit, L.; Jouber, L.; Maldivi, P ; Adamo, C. *J. Am. Chem. Soc.* **2006**, *128,* 2190.

(3) (a) Noury, S.; Krokidis, X.; Fuster, F.; Silvi, B. *TopMod Package*; Paris, 1997. (b) Noury, S.; Krokidis, X.; Fuster, F.; Silvi, B. *Computers and Chemistry*. 1999, *23*, 597.

(4) MOLEKEL 4.3 visualization package. CSCS, Swiss National Supercomputing Centre. http://www.cscs.ch/molekel/

(5) Bader, R. F. Atoms in molecules. A quantum theory. Clarendon, Oxford, **1990**.

(6) (a) Reed, A. E.; Weinhold, F. *J. Chem. Phys,* **1985**, *83*, 1736. (b) Reed, A. E.; Curtiss, L. A. ; Weinhold, F. *Chem. Rev.* **1988**, 88, 899.

(7) Clark, A.E.; Sonnenberg, J.L.; Hay, P.J.; Martin, R. L. *J. Chem. Phys,* **2004**, *121*, 2563.

(8) See for instance, (a) Ismail, N.; Heully, J.-L.;Saue, T.; Daudey, J.-P.; Marsden, C.J. *Chem. Phys. Lett.,* **1999***, 300,* 296. (b) Zhang, Z.; Pitzer, R.M. *J. Chem. Phys. A.,* **1999**, *103*, 6880. (c) Zhou, M.; Andrews, L.; Ismail, N. ; Marsden C. *J. Phys. Chem. A,* **2000***, 104,* 5495. (d) Matsika, S.; Zhang, Z.; Brozell, S.R.; Blaudeau, J.-P.; Wang, Q.M; Pitzer, R.M. *J. Phys.Chem.A.,* **2001**, *105*, 3825. (e) Gagliardi, L.; Roos, B.O.; Malmqvist, P-Å.; Dyke, J.M. *J. Phys. Chem. A,* **2001***, 105,* 10602. (f) de Jong, W.A. ; Harrison, R.J. ; Nichols, J.A. ; Dixon, D. A. *Theor. Chem. Acc.* **2001**, *107*, 22. (g Majumdar, D.; Balasubramanian, K.; Nitsche, H. *Chem. Phys. Lett.,* **2002***, 361,* 143. (h) Belanzoni, P.; Baerends, E. J.; Van Lenthe, E., *Mol. Phys.* **2005***, 103,* 775. (i) Moskaleva, L.V.; Matveev, A.V.; Krüger, S; Rösch, N. *Chem. Eur. J.,* **2006**, *12*, 629.

(9) Krokidis, X.; Goncalves, V.; Savin, A.; Silvi, B. *J. Phys. Chem. A,* **1998***, 102,* 5065.

(10) Gaussian 03, Revision C.02, Frisch, M. J.; Trucks, G. W.; Schlegel, H. B.; Scuseria, G. E.; Robb, M. A.; Cheeseman, J. R.; Montgomery, Jr., J. A.; Vreven, T.; Kudin, K. N.; Burant, J. C.; Millam, J. M.; Iyengar, S. S.; Tomasi, J.; Barone, V.; Mennucci, B.; Cossi, M.; Scalmani, G.; Rega, N.; Petersson, G. A.; Nakatsuji, H.; Hada, M.; Ehara, M.; Toyota, K.; Fukuda, R.; Hasegawa, J.; Ishida, M.; Nakajima, T.; Honda, Y.; Kitao, O.; Nakai, H.; Klene, M.; Li, X.; Knox, J. E.; Hratchian, H. P.; Cross, J. B.; Bakken, V.; Adamo, C.; Jaramillo, J.; Gomperts, R.; Stratmann, R. E.; Yazyev, O.; Austin, A. J.; Cammi, R.; Pomelli, C.; Ochterski, J. W.; Ayala, P. Y.; Morokuma, K.; Voth, G. A.; Salvador, P.; Dannenberg, J. J.; Zakrzewski, V. G.; Dapprich, S.; Daniels, A. D.; Strain, M. C.; Farkas, O.; Malick, D. K.; Rabuck, A. D.; Raghavachari, K.; Foresman, J. B.; Ortiz, J. V.; Cui, Q.; Baboul, A. G.; Clifford, S.; Cioslowski, J.; Stefanov, B. B.; Liu, G.; Liashenko, A.; Piskorz, P.; Komaromi, I.; Martin, R. L.; Fox, D. J.; Keith, T.; Al-

Laham, M. A.; Peng, C. Y.; Nanayakkara, A.; Challacombe, M.; Gill, P. M. W.; Johnson, B.; Chen, W.; Wong, M. W.; Gonzalez, C.; and Pople, J. A.; Gaussian, Inc., Wallingford CT, 2004.

Table S1 Average basin Population, $\bar{N}_i$, relative fluctuations, $\lambda(\bar{N}_i)$ and integrated spin densities, $<S_Z>$, (in electrons) of the key minima found along of the reaction path of $UO^+(^4\Delta)$ and H_2O (species involved in Path A) .

Basin	**UO^+ ($^4\Delta$)**		**I (^{4}A)**		**TS1 (^{4}A)**		**II (^{2}A)**		TS2 **(^{2}A)**		**III (^{2}A)**		**UO_2^+ ($^2\Phi_u$)**	
	$\bar{N}_i$ [$<S_Z>$]	$\lambda(\bar{N}_i)$	$\bar{N}_i$ [$<S_Z>$]	$\lambda(\bar{N}_i)$	$\bar{N}_i$ [$<S_Z>$]	$\lambda(\bar{N}_i)$	$\bar{N}_i$ [$<S_Z>$]	$\lambda(\bar{N}_i)$	$\bar{N}_i$ [$<S_Z>$]	$\lambda(\bar{N}_i)$	$\bar{N}_i$ [$<S_Z>$]	$\lambda(\bar{N}_i)$	$\bar{N}_i$ [$<S_Z>$]	$\lambda(\bar{N}_i)$
C(U)	18.86 [0.57]	0.17	17.94[0.50]	0.19	17.54[0.39]	0.19	17.64[0.21]	0.18	17.76[0.21]	0.18	17.84[0.20]	0.18	17.83[0.20]	0.18
V(U)	10.57[0.94]	0.65	11.52[0.99]	0.72	11.36[0.71]	0.74	10.75[0.28]	0.73	10.52[0.36]	0.75	10.20[0.33]	0.71	10.20[0.33]	0.77
$C(O_1)$	2.10	0.16	2.11	0.16	2.10	0.16	2.11	0.16	2.11	0.16	2.11	0.16	2.11	0.16
$C(O_2)$	-	-	2.11	0.16	2.11	0.16	2.11	0.16	2.11	0.16	2.11	0.16	2.11	0.16
$V(O_2,H_1)$	-	-	1.74	0.46	-	-	-		-	-	-	-	-	-
$V(O_2,H_2)$	-	-	1.73	0.46	1.81	0.46	1.76	0.46	0.65	0.76	-	-	-	-
$V(O_2)$	-	-	2.12	0.49	2.81	0.47	5.66	0.37	-	-	-	-	-	-
$V(O_2)$	-	-	2.25	0.50	2.78	0.47	-	-	-	-	-	-	-	-
$V(U,O_1)$	7.47	0.18	7.27	0.18	7.36	0.19	7.25[-0.02]	0.19	7.32	0.19	7.39[-0.01]	0.19	7.35	0.19
$V(U,O_1)\|U^1$	0.61	-	0.38	-	0.56		0.60		0.23	-	0.65		0.64	-
$V(U,O_2)$	-	-	-	-	-	-	-	-	6.21	0.26	7.39[-0.01]	0.19	7.40	0.19
$VU,O_2)\|U^1$	-	-	-	-	-		-	-	0.65	-	0.64		0.66	-
$V(H_1,U,O_2)$	-	-	-	-	1.11[0.33]	0.35	-	-	-	-	-	-	-	-
$V(H_1,U)$	-	-	-	-	-	-	1.69[-0.02]	0.31	1.66	0.33	-	-	-	-
$V(H_1,U)\|\ U^1$	-	-	-	-	-	-	0.30	-	0.26	-	-	-	-	-
$V(H_1,H_2)$	-	-	-	-	-	-	-	-	-	-	1.95	0.07	-	-

[1] V(U,X |U means atomic contribution from U atom to the V(U,X) valence basin.

Table S2 Average basin Population, $\bar{N}_i$, relative fluctuations, $\lambda(\bar{N}_i)$ and integrated spin densities, $\langle S_Z \rangle$, (in electrons) of the key minima found along of the reaction path of $UO^+(^4\Delta)$ and H_2O (species involved in Path B)

Basin	**TS3 (^{4}A'')**		IV **(^{4}A)**		**TS5 (^{2}A)**	
	$\bar{N}_i$ [$\langle S_Z \rangle$]	$\lambda(\bar{N}_i)$	$\bar{N}_i$ [$\langle S_Z \rangle$]	$\lambda(\bar{N}_i)$	$\bar{N}_i$ [$\langle S_Z \rangle$]	$\lambda(\bar{N}_i)$
C(U)	17.61 [0.50]	0.19	17.58 [0.51]	0.19	17.51 [0.34]	0.19
V(U)	12.07 [1.01]	0.71	12.03 [0.99]	0.72	11.72 [0.52]	0.71
$C(O_1)$	2.11	0.16	2.11	0.16	2.11	0.16
$C(O_2)$	2.11	0.16	2.14	0.16	2.12	0.16
$V(O_2,H_1)$	1.74	0.47	1.78	0.46	-	-
$V(O_1,H_2)$	-	-	1.84	0.46	-	-
$V(O_2)$	2.15	0.51	5.68	0.26	5.72	0.26
$V(O_2)$	2.17	0.51	-	-	-	-
$V(O_2)$	1.48	0.60	-	-	-	-
$V(O_1)$	-	-	5.79	0.25	-	-
$V(U,O_1)$	6.30 [-0.02]	0.24	-	-	-	-
$V(U,O_1)\|U^1$	0.16	-	-	-	-	-
$V(U,O_2)$	-	-	-	-	6.78	0.21
$VU,O_2)\|U^1$	-	-	-	-	0.16	-
$V(H_1,U,O_2)$	-	-	-	-	1.22	0.49
$V(H_2)$	0.37	0.85	-	-	-	-

Table S3 Average basin Population, $\bar{N}_i$, relative fluctuations, $\lambda(\bar{N}_i)$ and integrated spin densities, $\langle S_Z \rangle$, (in electrons) of the key minima found along of the reaction path of UO^{2+} ($^3\Sigma_g$) and H_2O (species involved in Path A) .

Basin	UO^{2+} ($^3\Sigma_g$)		I' (^{3}A)		TS1' (^{3}A)		II' (^{3}A)		TS2' (^{1}A)		III'(^{1}A)		UO_2^{2+} ($^1\Sigma_g$)	
	$\bar{N}_i$ [$\langle S_Z \rangle$]	$\lambda(\bar{N}_i)$	$\bar{N}_i$ [$\langle S_Z \rangle$]	$\lambda(\bar{N}_i)$	$\bar{N}_i$ [$\langle S_Z \rangle$]	$\lambda(\bar{N}_i)$	$\bar{N}_i$ [$\langle S_Z \rangle$]	$\lambda(\bar{N}_i)$	$\bar{N}_i$	$\lambda(\bar{N}_i)$	$\bar{N}_i$	$\lambda(\bar{N}_i)$	$\bar{N}_i$	$\lambda(\bar{N}_i)$
C(U)	17.61[0.39]	0.16	17.65 [0.39]	0.16	17.60 [0.25]	0.18	17.58 [0.21]	0.18	17.76	0.16	17.94	0.17	19.11	0.16
V(U)	11.09[0.63]	0.74	11.09 [0.62]	0.66	10.73 [0.45]	0.73	10.68 [0.37]	0.70	9.77	0.73	9.48	0.76	8.09	0.43
C(O_1)	2.10	0.16	2.12	0.16	2.11	0.16	2.11	0.16	2.11	0.16	2.11	0.16	2.11	0.16
C(O_2)	-	-	2.11	0.16	2.12	0.16	2.11	0.16	2.11	0.16	2.11	0.16	2.11	0.16
V(O_2,H_1)	-	-	1.74	0.45	-	-	-	-	-	-	-	-	-	-
V(O_2,H_2)	-	-	1.73	0.45	1.84	0.45	1.78	0.20	0.61	0.21	-	-	-	-
V(O_2)	-	-	2.15	0.49	2.65 [0.03]	0.49	5.56	0.28	-	-	-	-	-	-
V(O_2)	-	-	2.16	0.49	2.72 [0.03]	0.49	-	-	-	-	-	-	-	-
V(U,O_1)	7.19[-0.04]	0.20	7.23 [-0.04]	0.20	7.23[-0.03]	0.20	7.14 [-0.01]	0.20	7.15	0.21	7.20	0.21	7.25	0.20
V(U,O_1)|U[1]	0.61	-	0.60	-	0.71	-	0.61	-	0.71	-	0.70	-	0.76	-
V(U,O_2)	-	-	-	-	-	-	-	-	7.00	0.28	7.21	0.21	7.31	0.20
V(U,O_1)|U[1]	-	-	-	-	-	-	-	-	0.49	-	0.70	-	0.83	-
V(H_1,U,O_2)	-	-	-	-	0.98 [0.26]	0.47			-	-	-	-	-	-
V(H_1)	-	-	-	-	-	-	0.91 [0.44]	0.16	-	-	-	-	-	-
V(H_1,U)	-	-	-	-	-	-	-	-	1.47	0.40	-	-	-	-
V(H_1,U)| U[1]	-	-	-	-	-	-	-	-	0.18	-	-	-	-	-
V(H_1,H_2)	-	-	-	-	-	-	-	-	-	-	1.93	0.38	-	-

[1] V(U,X |U means atomic contribution from U atom to the V(U,X) valence basin.

Table S4 Average basin Population, $\bar{N}_i$, relative fluctuations, $\lambda(\bar{N}_i)$ and integrated spin densities, $\langle S_Z \rangle$, (in electrons) of the key minima found along of the reaction path of $UO^{2+}(^3\Sigma_g)$ and H_2O (species involved in Path A) .

Basin	**TS3 (^{3}A'')**		IV' **(^{3}A)**		**TS5 (^{3}A)**	
	$\bar{N}_i$ [$\langle S_Z \rangle$]	$\lambda(\bar{N}_i)$	$\bar{N}_i$ [$\langle S_Z \rangle$]	$\lambda(\bar{N}_i)$	$\bar{N}_i$ [$\langle S_Z \rangle$]	$\lambda(\bar{N}_i)$
C(U)	17.48 [0.38]	0.19	17.44 [0.38]	0.19	17.51 [0.34]	0.19
V(U)	10.49 [0.65]	0.72	11.62 [0.61]	0.72	11.72 [0.52]	0.71
$C(O_1)$	2.11	0.16	2.14	0.16	2.11	0.16
$C(O_2)$	2.12	0.16	2.14	0.16	2.12	0.16
$V(O_2,H_1)$	1.77	0.46	1.88	0.45	-	-
$V(O_1,H_2)$	-	-	1.89	0.45	-	-
$V(O_2)$	2.15	0.51	5.39	0.28	5.72	0.26
$V(O_2)$	2.17	0.51	-	-	-	-
$V(O_2)$	1.55	0.59	-	-	-	-
$V(O_1)$	-	-	5.45	0.28	-	-
$V(U,O_1)$	5.96 [-0.03]	0.27	-	-	-	-
$V(U,O_1)\|U^1$	0.17		-	-	-	-
$V(U,O_2)$	-	-	-	-	7.08	0.22
$VU,O_2)\|U^1$	-	-	-	-	0.59	-
$V(H_1,U,O_2)$	-	-	-	-	0.93	0.40
$V(H_2)$	0.39	0.85	-	-	-	-

Table S5 Bond Critical Point (3, -1) data (in atomic units) for all the species involved in the $UO^+ + H_2O$ reaction pathway (Path A).[1]

Bond	**UO^+** ($^4\Delta$)		**I** (^4A)		**TS1** (^4A)		**II** (^2A)		**TS2** (^2A)		**III** (^2A)		**UO_2^+** ($^2\Phi_u$)	
	ρ(bcp)	$\nabla^2\rho$(bcp)	ρ(bcp)	$\nabla^2\rho$(bcp)	ρ(bcp)	$\nabla^2\rho$(bcp)	ρ(bcp)	$\nabla^2\rho$(bcp)	ρ(bcp)	$\nabla^2\rho$(bcp)	ρ(bcp)	$\nabla^2\rho$(bcp)	ρ(bcp)	$\nabla^2\rho$(bcp)
U - O(1)	0.272	0.393	0.262	0.435	0.286	0.316	0.317	0.187	0.316	0.225	0.310	0.240	0.314	0.232
U - O(2)	-	-	0.048	0.200	0.118	0.465	0.162	0.461	0.223	0.275	0.310	0.240	0.314	0.232
O(2) – H(1)	-	-	0.351	-2.526	0.052	0.102	-	-	-	-	-	-	-	-
O(2) – H(2)	-	-	0.353	-2.526	0.347	-2.470	0.336	-2.419	0.216	-0.681	-	-	-	-
U – H(1)	-	-	-	-	-	-	0.116	-0.070	0.081	0.060	0.023	0.075	-	-
H(1) – H(2)	-	-	-	-	-	-			0.081	-0.031	0.254	-1.010	-	-

[1] H_2O O-H bond values : ρ(bcp) = 0.366 a.u , $\nabla^2\rho$(bcp) = -2.49 a.u. ; H_2 H-H bond values: ρ(r)= 0.261 a.u., $\nabla^2\rho$(bcp) =-1.056 a.u.

Table S6 Bond Critical Point (3, -1) data (in atomic units) for all the species involved in the $UO^+ + H_2O$ reaction pathway (Path B)[1]

Bond	**TS3** ($^4A''$)		**IV** (^4A)		**TS5** (^2A)	
	ρ(bcp)	$\nabla^2\rho$(bcp)	ρ(bcp)	$\nabla^2\rho$(bcp)	ρ(bcp)	$\nabla^2\rho$(bcp)
U - O(1)	0.205	0.415	0.137	0.520	0.141	0.527
U - O(2)	0.077	0.319	0.137	0.520	0.237	0.385
O(1) – H(2)	0.148	-0.126	0.351	-2.480	0.345	-2.466
O(2) – H(1)	0.351	-2.480	0.351	-2.480	0.108	0.061
O(2) – H(2)	0.158	-0.192	-	-	-	-
U – H(1)	0.051	0.268	-	-	-	-

[1] H_2O O-H bond values : ρ(bcp) = 0.366 a.u , $\nabla^2\rho$(bcp) = -2.49 a.u.

Table S7 Bond Critical Point (3, -1) data (in atomic units) for all the species involved in the UO^{2+} + H_2O reaction pathway(Path A).[1]

Bond	UO^{2+} ($^3\Sigma_g$)		I' (^{3}A)		TS1' (^{3}A)		II' (^{3}A)		TS2' (^{1}A)		III'(^{1}A)		UO_2^{2+} ($^1\Sigma_g$)	
	ρ(bcp)	$\nabla^2\rho$(bcp)	ρ(bcp)	$\nabla^2\rho$(bcp)	ρ(bcp)	$\nabla^2\rho$(bcp)	ρ(bcp)	$\nabla^2\rho$(bcp)	ρ(bcp)	$\nabla^2\rho$(bcp)	ρ(bcp)	$\nabla^2\rho$(bcp)	ρ(bcp)	$\nabla^2\rho$(bcp)
U - O(1)	0.332	0.281	0.319	0.294	0.338	0.192	0.340	0.151	0.362	0.225	0.364	0.284	0.368	0.282
U - O(2)	-	-	0.062	0.246	0.145	0.441	0.181	0.501	0.275	0.239	0.364	0.284	0.368	0.282
O(2) – H(1)	-	-	0.337	-2.460	0.075	0.084	-	-	0.064	0.163	-	-	-	-
O(2) – H(2)	-	-	0.338	-2.461	0.313	-2.309	0.309	-2.270	0.193	-0.540	-	-	-	-
U – H(1)	-	-	-	-	-	-	0.020	0.027	0.096	-0.017	0.032	0.077	-	-
H(1) – H(2)	-	-	-	-	-	-	-	-	0.080	-0.031	0.243	-0.949	-	-

[1] H_2O O-H bond values : ρ(bcp) = 0.366 a.u. , $\nabla^2\rho$(bcp) = -2.49 a.u. ; H_2 H-H bond values : ρ(r)= 0.261 a.u. $\nabla^2\rho$(bcp) = -1.056 a.u.

Table S8 Bond Critical Point (3, -1) data (in atomic units) for all the species involved in the UO^{2+} + H_2O reaction pathway (Path B)[1]

Bond	TS3' (^{3}A'')		IV' (^{3}A)		TS5 '(^{3}A)	
	ρ(bcp)	$\nabla^2\rho$(bcp)	ρ(bcp)	$\nabla^2\rho$(bcp)	ρ(bcp)	$\nabla^2\rho$(bcp)
U - O(1)	0.250	0.300	0.167	0.586	0.179	0.527
U - O(2)	0.113	0.415	0.167	0.586	0.306	0.239
O(1) – H(2)	0.157	-0.267	0.323	-2.370	0.311	-2.290
O(2) – H(1)	0.326	-2.383	0.323	-2.370	0.059	0.087
O(2) – H(2)	0.124	-0.015			-	-
U – H(1)	0.059	0.300	-	-	-	-

[1] H_2O O-H bond values : ρ(bcp) = 0.366 a.u , $\nabla^2\rho$(bcp) = -2.49 a.u.

Table S9 Ratio of atomic radii (r_c/r_a) of the uranium mono- and dioxide cations determined from a) the position of the bond critical points computed by AIM and b) the ratio of AIM basin volumes, as calculated byTopMod package.

Species	U-BCP/O-BCP[1]	Atomic radii ratio(a)	Atomic radii ratio(b)
$U(III)O^+$ (4)	0.983 / 0.811	1.21	1.24
$U(IV)O^{2+}$ (3)	0.953 / 0.800	1.19	1.17
$U(V)O_2^+$ (2)	0.791 / 0.969	0.82	1.05
$U(VI)O_2^{2+}$ (1)	0.940 /0.757	1.24	1.08

[1]U-BCP: distance (in Å) between the BCP and the Uranium atom, O-BCP: distance (in Å) between the BCP and the oxygen atom.

Table S10 Calculated AIM Uranium charges, $q(U)^{AIM}$, natural population analysis (NPA)[1] charges, q(X), and metal valence populations for all the lowest-energy spin state species involved in the $UO^+ + H_2O$ pathway. The spin state is given in parentheses.

Species (Spin Multiplicity)	$q(U)^{AIM}$	q(U)	$q(O_1)$	$q(O_2)$	$q(H_1)$	$q(H_2)$	Metal valence populations		
							7s	5f	6d
U^+ [Rn] $5f^3$ $7s^2$ (4)	-	1.00	-	-	-	-	2.00	3.00	-
H_2O (1)	-	-	-	-0.91	0.46	0.46	-	-	-
UO^+ (4)	1.98	2.18	-1.18	-	-	-	0.11	3.09	0.62
UO-H_2O^+ (4)	1.94	2.19	-1.21	-1.03	0.53	0.53	0.15	3.13	0.51
TS1 (4)	2.45	2.64	-1.01	-1.15	-0.01	0.54	0.08	2.88	0.44
HUO_2H^+ (2)	2.62	2.85	-0.85	-1.10	-0.46	0.56	0.20	2.65	0.48
TS2 (2)	2.65	2.77	-0.84	-0.92	-0.40	0.40	0.16	2.79	0.45
$(H_2)UO_2^+$ (2)	2.66	2.76	-0.89	-0.89	0.01	0.01	0.07	2.98	0.42
UO_2^+ (2)	2.69	2.79	-0.89	-0.89	-	-	0.06	2.97	0.42
UO_2H^+ (3)	2.48	2.64	-0.98	-1.20	-	-	0.04	3.13	0.33
TS3 (4)	2.13	2.34	-1.20	-1.20	0.51	0.54	0.07	3.15	0.44
$U(OH)_2^+$(4)	2.25	2.47	-1.27	-1.27	0.53	0.53	0.10	3.15	0.29
TS5 (2)	2.40	2.60	-0.96	-1.20	0.03	0.54	0.15	2.84	0.43

[1] Calculated using the default atomic orbital partitioning as implemented in Gaussian03. Valence/Rydberg partition: [7s 5f]/8s-10s 7p-10p 6d-9d 6f 7f]

Table S11 Natural population analysis (NPA)[1] charges, q(X), and metal valence populations for all the lowest-energy spin state species involved in the $UO^+ + H_2O$ pathway. The spin state is given in parentheses.

Species (Spin Multiplicity)	q(U)	$q(O_1)$	$q(O_2)$	$q(H_1)$	$q(H_2)$	Metal valence populations		
						7s	5f	6d
U^+ [Rn] $5f^3$ $7s^2$ (4)	1.00	-	-	-	-	2.00	3.00	-
H_2O (1)	-	-	-0.91	0.46	0.46	-	-	-
UO^+ (4)	2.00	-1.00	-	-	-	-	3.31	0.75
UO-H_2O^+ (4)	1.93	-0.99	-0.99	0.53	0.53	0.16	3.13	0.83
TS1 (4)	2.21	-0.77	-1.02	0.04	0.54	0.08	2.89	0.92
HUO_2H^+ (2)	2.23	-0.58	-0.93	-0.28	0.55	0.21	2.66	1.08
TS2 (2)	2.20	-0.59	-0.75	-0.28	0.41	0.15	2.79	1.01
$(H_2)UO_2^+$ (2)	2.23	-0.58	-0.93	-0.28	0.55	0.21	2.66	1.08
UO_2^+ (2)	2.33	-0.66	-0.66	-	-	0.04	2.97	0.92
UO_2H^+ (3)	2.30	-0.77	-1.07	0.54	-	0.03	3.13	0.68
TS3 (4)	2.10	-1.03	-1.13	0.52	0.54	0.09	3.15	0.71
$U(OH)_2^+$(4)	2.18	-1.12	-1.12	0.53	0.53	0.11	3.15	0.61
TS5 (2)	2.09	-0.73	-1.01	0.11	0.55	0.21	2.76	1.01

[1] Calculated using the modified atomic orbital partitioning. Valence/Rydberg partition: [7s 5f 6d] / 8s -10s 7p -10p 7d -9d 6f 7f]

Table S12 Calculated AIM Uranium charges, $q(U)^{AIM}$, natural population analysis (NPA)[1] charges, q(X), and metal valence populations for all the lowest-energy spin state species involved in the $UO^{2+} + H_2O$. The spin state is given in parentheses.

Species (Spin Multiplicity)	$q(U)^{AIM}$	q(U)	$q(O_1)$	$q(O_2)$	$q(H_1)$	$q(H_2)$	Metal valence populations		
							7s	5f	6d
U^{+2} [Rn] $5f^4$ (5)	-	2.00	-	-	-	-	-	4.00	-
H_2O (1)	-	-	-	-0.91	0.46	0.46	-	-	-
UO^{+2} (3)	2.70	2.87	-0.87	-	-	-	-	2.74	0.13
UO-H_2O^{+2} (3)	2.61	2.85	-0.91	-1.06	0.56	0.56	0.02	2.73	0.44
TS1' (3)	2.80	2.92	-0.70	-1.02	0.18	0.62	0.09	2.74	0.37
HUO_2H^{+2} (3)	2.87	3.02	-0.70	-1.04	0.11	0.63	0.08	2.72	0.37
TS2' (1)	3.01	3.10	-0.62	-0.75	0.19	0.45	0.13	2.56	0.49
$(H_2)UO_2^{+2}$ (1)	3.13	3.24	-0.65	-0.65	0.03	0.03	0.08	2.52	0.49
UO_2^{+2} (1)	3.20	3.30	-0.65	-0.65	-	-	0.06	2.51	0.38
UO_2H^{+2} (2)	2.97	3.11	-0.69	-1.04	0.62	-	0.03	2.74	0.34
TS3' (3)	2.74	2.95	-0.94	-1.16	0.54	0.60	0.03	2.66	0.40
$U(OH)_2^{2+}$ (3)	2.82	3.05	-1.12	-1.12	0.59	0.59	0.03	2.61	0.34
TS5' (3)	2.83	2.97	-0.72	-1.05	0.19	0.61	0.08	2.74	0.36

[1] Calculated using the default atomic orbital partitioning as implemented in Gaussian03. Valence/Rydberg partition: [7s 5f]/8s-10s 7p-10p 6d-9d 6f 7f]

Table S13 Natural population analysis (NPA)[1] charges, q(X), and metal valence populations for all the lowest-energy spin state species involved in the UO^{2+} + H_2O. The spin state is given in parentheses.

Species (Spin Multiplicity)	q(U)	$q(O_1)$	$q(O_2)$	$q(H_1)$	$q(H_2)$	Metal valence populations		
						7s	5f	6d
U^{+2} [Rn] $5f^4$ (5)	2.00	-	-	-	-	-	4.00	-
H_2O (1)	-	-	-0.91	0.46	0.46	-	-	-
UO^{+2} (3)	2.71	-0.71	-	-	-	-	2.56	0.80
UO-H_2O^{+2} (3)	2.60	-0.72	-1.01	0.57	0.57	0.03	2.75	0.72
TS1' (3)	2.54	-0.49	-0.90	0.23	0.62	0.08	2.75	0.77
HUO_2H^{+2} (3)	2.59	-0.48	-0.88	0.15	0.61	0.06	2.73	0.82
TS2' (1)	2.52	-0.37	-0.55	0.06	0.45	0.12	2.55	1.07
$(H_2)UO_2^{+2}$ (1)	2.69	-0.40	-0.40	0.06	0.06	0.06	2.51	1.07
UO_2^{+2} (1)	2.83	-0.41	-0.41	-	-	0.03	2.50	1.00
UO_2H^{+2} (2)	2.74	-0.48	-0.88	0.62	-	0.02	2.61	0.78
TS3' (3)	2.68	-0.77	-1.06	0.55	0.60	0.04	2.67	0.68
$U(OH)_2^{2+}$ (3)	2.70	-0.95	-0.95	0.59	0.59	0.03	2.61	0.72
TS5' (3)	2.58	-0.53	-0.89	0.22	0.61	0.06	2.74	0.76

[1] Calculated using the modified atomic orbital partitioning. Valence/Rydberg partition: [7s 5f 6d] / 8s -10s 7p -10p 7d -9d 6f 7f]

Table S14 Total $<S^2>$ values for all the species involved in the $UO^+ + H_2O$ reaction path. The spin state is given in parentheses.

Species	PW91/ZORA	B3LYP/SDD	
	$<S^2>$	$<S^2>$	$<S^2>_A$ [1]
$UO^+(2)$	1.75	1.75	0.76
$UO^+(4)$	3.76	3.76	3.75
UO^+-$H_2O(2)$	1.75	0.77	0.75
UO^+-$H_2O(4)$	3.76	3.77	3.75
TS1 (2)	1.28	1.57	0.78
TS1(4)	3.77	3.77	3.75
HUO_2H^+ (2)	0.76	0.77	0.75
HUO_2H^+ (4)	3.76	3.77	3.75
TS2 (2)	0.75	0.75	0.75
TS2 (4)	3.76	-	-
$H_2UO_2^+$ (2)	0.75	0.76	0.75
$H_2UO_2^+$ (4)	3.76	3.76	3.75
UO_2^+ (2)	0.75	0.76	0.75
UO_2^+ (4)	3.76	3.76	3.75
HUO_2^+ (3)	2.01	2.01	2.00
TS3 (4)	3.76	3.76	3,.75
TS3(2)	1.76	1.75	0.76
$U(OH)_2^+$ (4)	3.76	3.75	3.75
$U(OH)_2^+$ (2)	1.75	1.55	0.78
TS5 (4)	3.76	3.76	3.75
TS5(2)	1.21	1.55	0.70

[1] $<S^2>_A$: Total S^2 value after annihilation of the first spin contaminant.

Table S15 Total $<S^2>$ values for all the species involved in the $UO^{2+} + H_2O$ reaction path. The spin state is given in parentheses.

Species	PW91/ZORA	B3LYP/SDD	
	$<S^2>$	$<S^2>$	$<S^2>_A$ [1]
UO^{+2} (3)	2.01	2.02	2.00
UO^{2+}-H_2O(3)	2.04	2.01	2.00
TS1'(3)	2.01	2.01	2.00
HUO_2H^{2+} (3)	2.05	2.00	2.00
TS2' (3)	-	-	-
$H_2UO_2^{+}$ (3)	2.00	2.00	2.00
UO_2^{2+} (3)	2.00	2.00	2.00
HUO_2^{2+} (2)	0.76	0.75	0.75
TS3' (3)	2.03	2.02	2.00
$U(OH)_2^{2+}$ (3)	2.02	2.00	2.00
TS5' (3)	2.02	2.02	2.00

[1] $<S^2>_A$: Total S^2 value after annihilation of the first spin contaminant.

The wavefunctions of UO^{2+}(1), UO^{2+}-H_2O (1) and TS1'(1) moieties present a singlet-triplet instability. The $<S^2>$ and $<S^2>_A$ values of the optimized wavefunction (stable=opt keyword of Gaussian03 program) were 1.00 and 0.01 for UO^{2+}(1); 1.02 and 0.01 for UO^{2+}-H_2O (1), and 1.02 and 0.05 for TS1'.

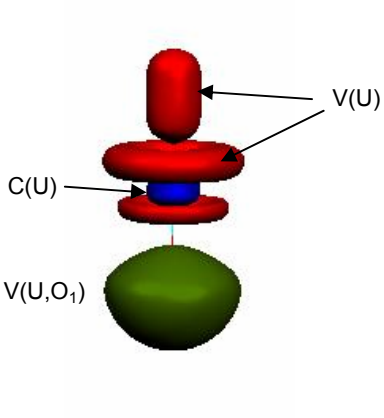

UO^{+} ($^{4}\Delta$)

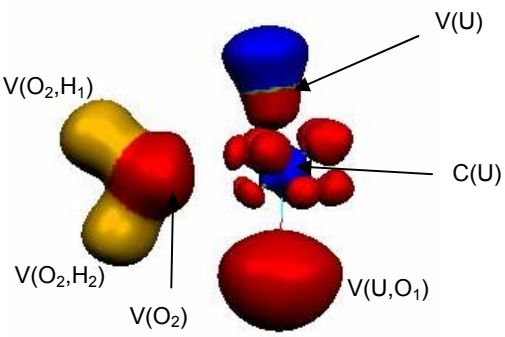

I (^{4}A)

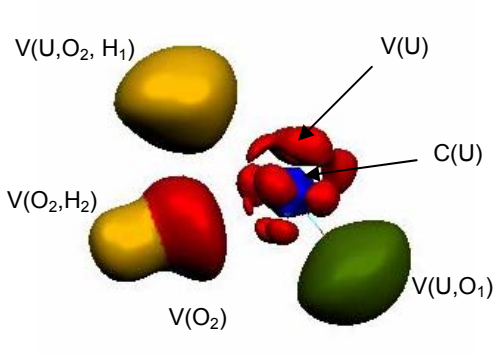

TS1 (^{4}A)

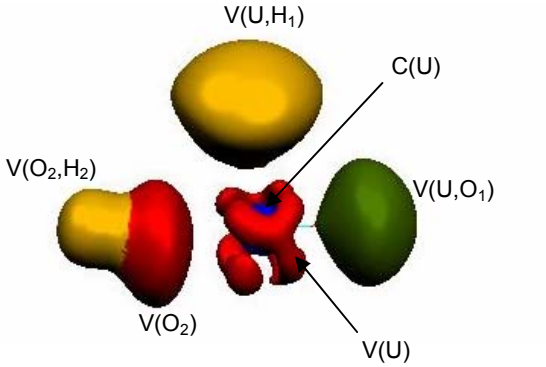

II (^{2}A)

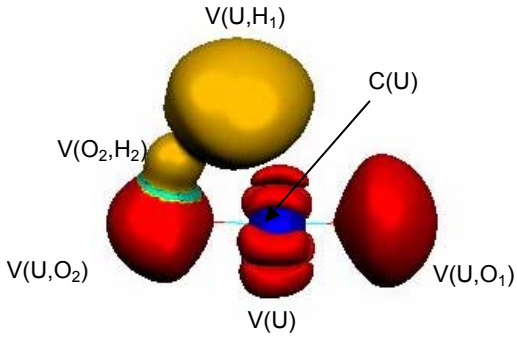

TS2 (^{2}A)

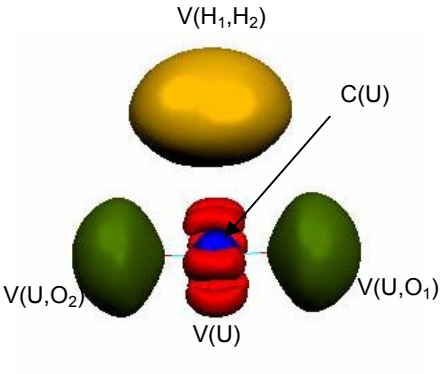

III (^{2}A)

Figure S1

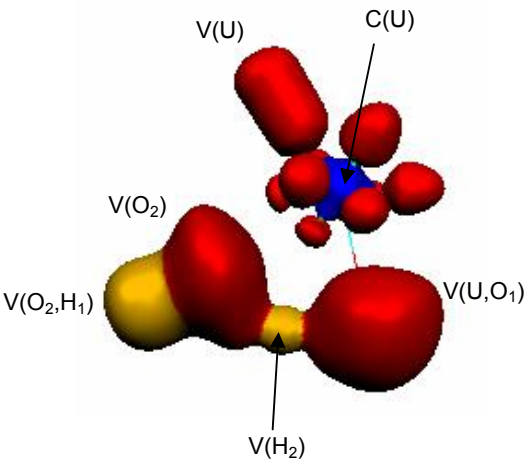

TS3 (^{4}A'')

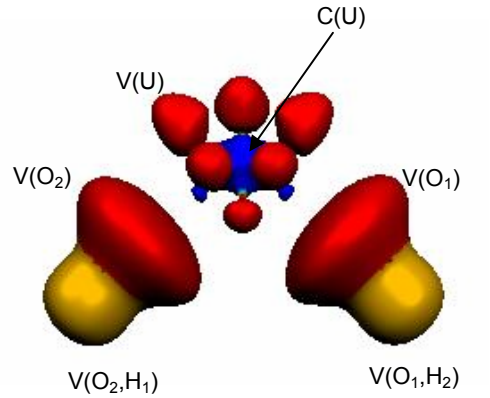

IV (^{4}A)

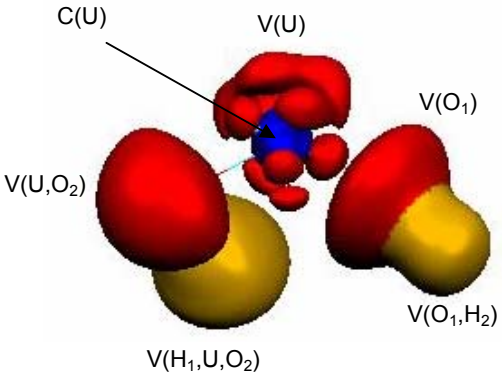

TS5 (^{2}A)

Figure S2

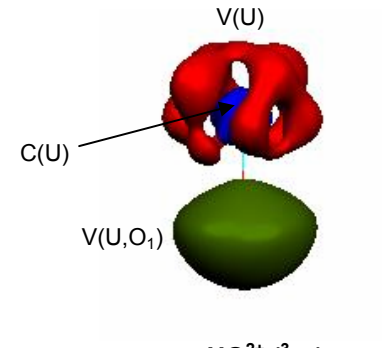

UO^{2+} ($^3\Sigma_g$)

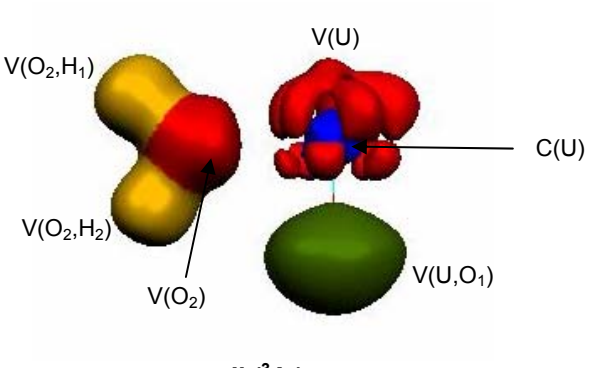

I' (^{3}A)

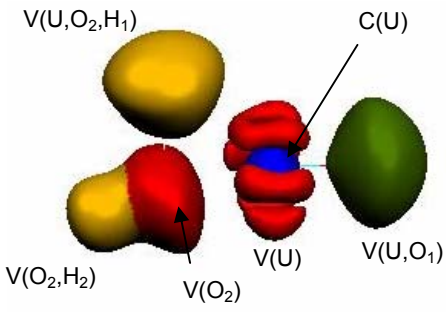

TS1' (^{3}A)

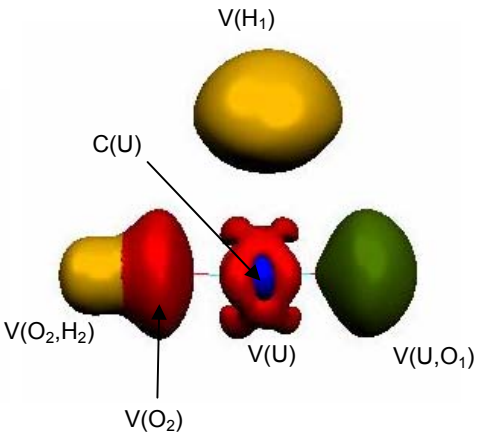

II' (^{3}A)

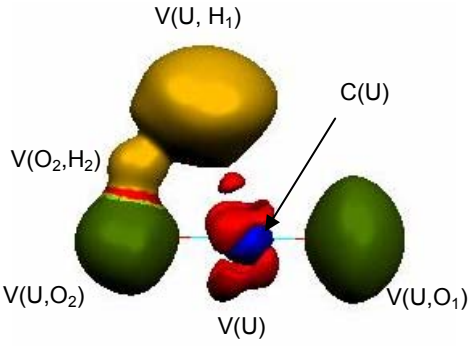

TS2' (^{1}A)

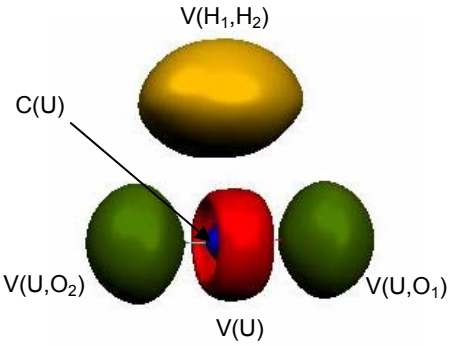

III' (^{1}A)

Figure S3

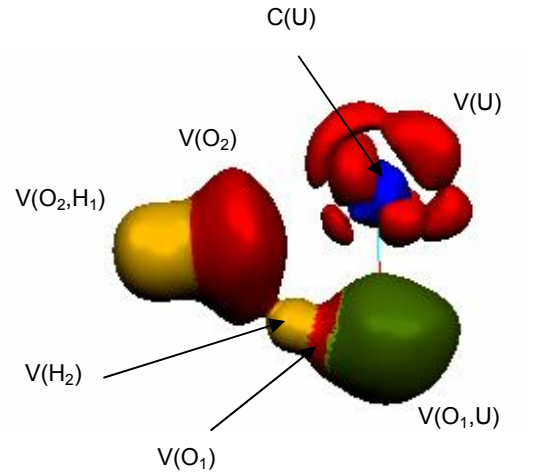

TS3' (^{3}A'')

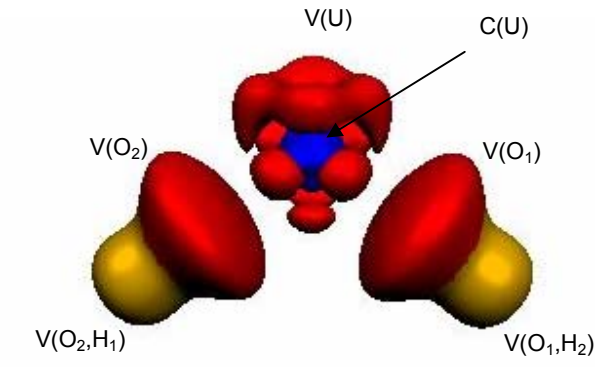

IV' (^{3}A)

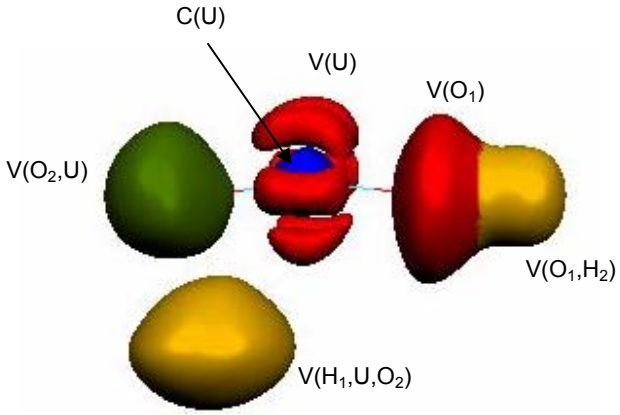

TS5' (^{3}A'')

Figure S4